USGS Grant Number: G15AP00058

Title: The role of seismically initiated CO_2 gas bubble growth in groundwater as a mechanism for remotely triggered seismicity

Authors: Jackson B. Crews[1] & Susan Rybarski[1]

[1]Division of Hydrologic Sciences

Desert Research Institute

2215 Raggio Parkway

Reno, Nevada 89512

e-mail: jcrews@dri.edu,

Telephone: 775-673-7605

Fax: 775-673-7363

Term covered: April 1, 2015 – March 31, 2017

Abstract

The purpose of this study is to evaluate whether or not and to what extent the growth or extinction of gas bubbles in groundwater is influenced by distant earthquakes, to document and quantify this effect, and to evaluate its potential to remotely trigger local earthquakes. Digital audio was recorded in a CO_2-enriched hydrothermal monitoring well in Long Valley Caldera, south of Mammoth Lakes, California, USA, known as Core-Hole 10B (CH-10B), which exhibits a co-seismic water level drop in response to seismic events around the Earth and resides in a region historically susceptible to remote seismic triggering by distant earthquakes. To further explore the possible connection between remotely triggered seismicity and gas bubble growth in groundwater, we compare the frequency content of the audio spectrum in the well before and after four major earthquakes, three of which initiated a water level response, and one that didn't. The acoustic power in the 200-300 Hz band (a proxy for the rupture rate of gas bubbles with a radius on the order of a few millimeters) increased after the arrival of the P-wave, and were followed by a change in water level. In contrast, no change in the audio spectrum occurred following the 19 Aug. 2016 M7.4 South Georgia Island earthquake, which did not cause the CH-10B water level to change, indicating no change in the rupture rate, size distribution, or number density of gas bubbles in the formation. The correspondence of the acoustic and water level responses at CH-10B indicates that CO_2 gas bubble growth and dissolution in groundwater, under the action of volumetric dilation or mechanical phase segregation of the formation fluid constituents by seismic waves, contributes to the co-seismic water level response at CH-10B. While the onset of the acoustic response is synched closely with the arrival of the P-wave, the water level response is delayed, and exhibits characteristics similar to results from prior benchtop laboratory experiments in Berea sandstone. The absence of the co-seismic acoustic response may arise from variations in the pre-seismic reservoir conditions – notably fluid compressibility, which is a strong function of gas-phase volume fraction in the formation fluid, in addition to the frequency content, bearing, and polarization of the seismic wave pulse arriving at CH-10B. Looking forward, acoustic

monitoring, with some additional refinement, could be used to measure gas flux from groundwater to the atmosphere, and to assess gas-phase volume fraction and bubble mobility in groundwater.

Introduction

Groundwater containing a high concentration of dissolved carbon dioxide (CO_2) gas is susceptible to rapid bubble nucleation and growth in response to dilational seismic wave propagation and post-seismic static stress drops. The nucleation and growth of CO_2 bubbles in a confined aquifer results in persistent excess pore fluid pressure, which is linked to remotely triggered seismicity. Laboratory studies conducted on a Berea sandstone core flooded with high-CO_2 water have shown that a rapid drop in confining stress results in a transient buildup of pore pressure with excess pressure on the order of 10^{-1} MPa, and an equilibration timescale of 10^{1} hours. When subjected to an oscillating confining stress representative of the dynamic stress produced by the June 28, 1992 M_w 7.3 Landers, California, earthquake Rayleigh wave as it traveled through Parkfield and Long Valley caldera, California, the resulting excess pore fluid pressure in the Berea sandstone core was equivalent in magnitude to borehole water level rises observed at both of those locations. These experimental results indicate that short-duration dilational seismic waves produce persistent excess pore fluid pressure, which reduces effective stress, potentially triggering movement in critically loaded geologic faults located hundreds or thousands of kilometers from an earthquake epicenter. This remote triggering mechanism is attractive because it addresses the time delay that is observed between the main shock and subsequent triggered events, separated in time by hours or days. Gas bubble growth in or near a critically loaded fault causes a localized increase in pore fluid pressure, which diffuses in space and time at a rate governed by the hydraulic diffusivity. Building on the results of those laboratory experiments, the next logical step is to establish the efficacy of this triggering mechanism in the field. To achieve this, instrumentation must be deployed to directly or indirectly detect the nucleation and growth of gas bubbles in groundwater. Acoustic detection of gas bubble rupture at the free surface in a wellbore, gas composition monitoring, and piezometric head measurements collocated with seismometers and borehole strain meters will enable resolution of the mechanism for remotely triggered seismicity in active geothermal and volcanic areas, which are associated with high concentrations of crustal CO_2.

Background

The mechanism by which short-duration, low-amplitude dynamic stress from a distant earthquake can trigger an increase in seismicity at distances on the order of 10^{3} km from the main shock is not well understood. Models and mechanisms for remote seismic triggering exist, but they do not explain why remotely triggered seismicity is delayed by hours or days following the main shock, or why triggered events tend to occur in locations associated with active geothermal reservoirs and recent volcanism. A growing body of evidence, comprised of field observations and laboratory experiments, suggests that seismically initiated carbon dioxide gas bubble nucleation and growth in a CO_2-rich confined aquifer can cause the pore fluid pressure to increase on a timescale that is consistent with the observed delay between remotely triggered seismicity and the main shock. Field investigations are proposed to resolve the influence of seismically initiated CO_2 gas bubble nucleation and growth as a mechanism for remotely triggered seismicity at Long Valley caldera, California.

Carbon dioxide in the Earth's crust

Carbon dioxide (CO_2) gas is associated with seismically active locations [e.g., *Lewicki and Brantley*, 2000; *Barnes et al*., 1984; *Irwin and Barnes*, 1980]. A large surficial release of CO_2 occurred during a seismic swarm at Long Valley caldera, California, in 1988 and 1989. Because CO_2 is denser than air, it sits on the land surface where it presents a suffocation hazard to humans and vegetation [*Bergfeld et al*.,

2006; *Farrar et al*., 1995]. Large surface fluxes of CO_2 are also reported in some geothermal sites including Dixie Valley, Nevada [*Bergfeld et al.*, 2001], where a 1954 earthquake caused every non-flowing well in the valley to flow under artesian pressure, flooding the valley with surface water [*Zones*, 1957]. Carbon dioxide derived from magma, metamorphism, and shallow biogenic processes can dissolve in groundwater [*Kerrick*, 2001, and references therein]. The solubility of CO_2 in water is a function of the pressure, temperature, pH, and salinity [*Diamond and Akinfiev*, 2003]. For groundwater that is initially saturated with respect to dissolved CO_2, a reduction in pore fluid pressure results in an instantaneously supersaturated condition, which causes some of the CO_2 dissolved in the water to come out of solution and appear as gas bubbles. Under confined conditions, newly formed CO_2 gas bubbles displace and compress the water in the pore space, resulting in elevated pore fluid pressure and reduced effective stress.

Dilational Seismic Waves

Dilational seismic waves (e.g. Rayleigh and P-waves) cause sinusoidal oscillation of the mean normal confining stress [*Lowrie*, 1997; *Geertsma and Smit*, 1961; *Biot*, 1956], which results in oscillation of the pore fluid pressure. If the pore fluid pressure falls below a critical threshold called the bubble pressure during some portion of the oscillation, CO_2 bubbles will form in the pore space. The rate at which CO_2 comes out of solution is several orders of magnitude faster than the rate at which gas-phase CO_2 dissolves in water; as a result, bubbles in the pore space re-dissolve slowly and persist after cessation of the seismic oscillation. Bubbles in the pore space compress and displace pore water, resulting in a persistent increase in pore fluid pressure and reduction of effective stress. This process is conceptualized in figures 1 and 2.

The saturation with respect to dissolved CO_2 is defined as the ratio of the CO_2 partial pressure, p_{CO_2}, to the pore pressure, p_p,

$$W = p_{CO_2} / p_p$$

The pressure at which bubble nucleation and growth begin is called the bubble pressure, p_b, which is a function of p_{CO_2}, the interfacial tension between CO_2 and H_2O, γ, and the radius of curvature, *R'*, of pre-existing gas cavities trapped in crevices on the mineral surface [*Jones et al.*, 1999],

$$p_b = p_{CO_2} + \frac{2\gamma}{R'}$$

The quantity $2\gamma / R'$ is the Laplace pressure, which is the difference in pressure between the inside and the outside of a bubble. Experiments conducted in a Berea sandstone core flooded with aqueous CO_2 at a partial pressure of 1.758 MPa (255 psig) indicate that the Laplace pressure is on the order of 0.1 MPa. Substituting $20 < \gamma < 50$ mN/m [*Nielsen et al.*, 2012], the mean radius of pre-existing gas cavities is 0.3 – 0.8 μm [*Crews and Cooper*, 2014a].

Remotely Triggered Seismicity

Seismicity remotely triggered by the June 28, 1992 M_w 7.3 Landers, California, earthquake occurred in areas associated with, but not limited to, active geothermal and volcanic sites, with time delays ranging from seconds to days [*Hill et al*., 1993]. Similarly, remotely triggered seismicity occurred in response to the 2002 Denali Fault earthquake at locations that were triggered by the Landers earthquake, including Yellowstone caldera, WY, Cedar City, UT, and the Coso volcanic field, 3,600 km from the epicenter,

with time delays ranging from hours to days between the main shock and induced events [*Hill and Prejean*, 2006; *Prejean et al*., 2004]. The Landers and Denali earthquakes triggered seismicity in the Long Valley caldera (LVC), California. Borehole strain instrumentation at LVC recorded dynamic stress oscillations in the 0.3-0.4 MPa amplitude range in the 0.05-0.30 Hz frequency band in response the Landers earthquake. The water level in the CW-3 well in LVC rose 41.8 cm in response to the Landers earthquake [*Roeloffs et al*., 1995], and this pore pressure increase may be linked to seismicity induced at LVC by the Landers main shock [*Hill et al.*, 1993; *Roeloffs et al.*, 1998]. Dynamic stress in the 0.2-0.3 MPa range in the same frequency band was recorded at Yellowstone caldera and Cedar City in response to a Rayleigh wave generated by the Denali earthquake [*Husen et al.*, 2004; *Pankow et al*., 2004]. Induced seismicity at LVC commenced 23.5 hours after the main shock [*Hill and Prejean*, 2006].

Experimental evidence for a triggering mechanism

A jacketed Berea sandstone core was flooded with an initially sub-saturated aqueous CO_2 solution and subjected to sinusoidal confining stress oscillations in the amplitude and frequency range of the Landers Rayleigh wave, as it passed through LVC. After six oscillation cycles, the confining stress $\bar{\sigma}$ was returned to its initial value, and the pore pressure p_p was compared to the dissolved-gas-free value expected based on poroelastic theory [*Skempton*, 1954],

$$p_p(\bar{\sigma}) = p_p^o + B(\bar{\sigma} - \bar{\sigma}_o)$$

where $B = \Delta p_p / \Delta \bar{\sigma}$ is Skempton's coefficient, a property of the liquid-saturated porous matrix, p_p^o is the initial pore fluid pressure, and $\bar{\sigma}_o$ is the initial mean normal confining stress. The excess pore fluid pressure caused by the growth of CO_2 bubbles in the pore space ranged from 16 – 60 cm of equivalent freshwater head. The magnitude of the measured response scaled with the confining stress oscillation amplitude and the oscillation frequency, as shown in figure 3.

Several mechanisms for remote seismic triggering have been proposed, including dynamic stress in the near field [*Gomberg et al*., 2003] and stress transfer during and after the main shock [*Freed*, 2005]. Candidate mechanisms generally point to diffusion of a localized, sudden increase in pore fluid pressure [e.g., *Jónsson et al*., 2003] that reduces effective stress and, thereby, reduces the critical shear stress required to initiate fault movement [*Hubbert and Rubey*, 1959],

$$\tau_{critical} = \mu(\bar{\sigma} - p_p) + \tau_o$$

Previously proposed mechanisms for remotely triggered seismicity are linked to seismically induced pore fluid pressure transients. Several mechanisms for co-seismic pore fluid pressure increases have been described in the literature, including permeability enhancement caused by dynamic stress and pore fluid pressure oscillation [*Elkhoury et al*., 2010, 2011; *Manga et al*., 2012; *Brodsky et al*., 2003], and gas bubble growth by rectified diffusion [*Sturtevant et al*., 1996, *Ichihara and Brodsky*, 2006; *Manga and Brodsky*, 2006]. Evidence supporting an increase in pore fluid pressure as the triggering mechanism is found in studies linking fluid injection to induced seismicity [e.g., *Ellsworth*, 2013]. Numerous instances of co-seismic borehole water level rise [e.g., *Roeloffs et al*., 1995] are reported at locations and times at which remotely triggered seismicity is also reported, suggesting that the two phenomena might be causally connected [*Roeloffs*, 1998]. In addition, some wells that exhibit co-seismic water level rises also host gas bubbles. Gas bubbles of unknown composition audibly rupture in the Bourdieu Valley well in Parkfield, California [*Roeloffs*, 1998], and municipal supply wells operated by the City of San Bernardino

began producing air bubbles slightly enriched with CO_2 after the 1992 Landers, California, earthquake [*Roeloffs et al*., 1995]. A conceptualization of remote seismic triggering caused by CO_2 gas bubble nucleation in and near a critically stressed fault is shown in Figure 4. The time delay between the main shock and induced seismic events may be the result of CO_2 gas bubble nucleation and growth distal to the fault. The pore fluid pressure increase caused by bubble nucleation at one location is not instantaneously communicated to all parts of the aquifer. The pore pressure increase diffuses in space and time according to the groundwater flow equation [*Bear*, 1988],

$$S_s \frac{\partial h}{\partial t} = \frac{\partial}{\partial x_i}\left(K_{ij} \frac{\partial h}{\partial x_j} \right)$$

where S_s is the specific storage (L^{-1}), h is hydraulic head, and K is the hydraulic conductivity. The solution was worked out in the context of heat conduction theory by *Carslaw and Jaeger* (1959), and the solution in one dimension is:

$$h(x,t) = \Delta h\left(1 - erf\left(\frac{x}{\sqrt{4K_x t / S_s}} \right) \right)$$

where Δh is a local head increase caused by bubble nucleation and growth. This solution is plotted for the case Δh = 1 m, S_s = 10^{-4} m^{-1}, K_x = 1 m/d, and x = 100 m in Figure 5. Seismicity is associated with zones of high local CO_2 flux, which has been attributed to fault weakening due to clay mineral deposition [*Weinlich*, 2014]. Seismically initiated CO_2 gas bubble nucleation and growth in such areas could function as a feedback mechanism on local seismicity. The extent to which the growth of gas bubbles drives local seismicity is dependent on the pre-earthquake saturation with respect to dissolved CO_2, which may be underestimated in conventional groundwater dissolved gas surveys due to degasing in the wellbore [*Roy and Ryan*, 2010].

The pore pressure spike has been speculatively linked to the exsolution and subsequent buoyant ascent of water vapor bubbles or carbon dioxide bubbles in a magma body [*Linde et al.*, 1994] and rapid permeability enhancement caused by ground shaking [*Elkhoury et al*., 2006; *Wang et al*., 2004]. While these mechanisms are viable, pore pressure buildup due to CO_2 gas bubble nucleation and growth in a confined aquifer in response to Rayleigh wave propagation and/or static stress reduction is particularly relevant in seismically active areas known to host an abundance of crustal CO_2, of which LVC is a prime example.

Site Selection, Physical Setting and Local Seismicity

Core Hole 10-B (CH-10B) is a USGS water-level monitoring well located south of Mammoth Lakes, CA, USA, inside Long Valley Caldera. A schematic of the well construction is shown in figure 6. The water temperature in the wellbore exceeds 100^{o}C. The wellhead resides inside a steel standing-room enclosure that houses a barometric-corrected gas-bubbler-based water level measurement system, data logger and a downhole thermistor array operated by the USGS. The depth to water is typically around 75 feet from the top of the casing, but is known to drop by a foot or more in response to M6+ earthquakes all over the Earth through a mechanism that is the subject of this investigation.

Instrumentation

The borehole fluid temperature presents the greatest challenge for instrumenting CH-10B and wells like it. The gas-bubble water level monitoring system was implemented after a custom-built pressure transducer failed to withstand the thermal load. A hydrophone rated to a maximum temperature of 120^{o}C was installed on June 18, 2015, approximately six feet below the water surface. The high-temperature-rated leads from the hydrophone were soldered to a shielded, Teflon-wrapped cable that terminated at an XLR jack on a Sound Devices ® 702 digital audio recorder. The audio signal from the hydrophone returned clear reports of the gas bubbler's regular periodic soundings in addition to higher-frequency bubbling noise. Between the hydrophone's fifth and sixth hour in the well, the signal turned to noise. The manufacturer had bench-tested the same model in pure water at 120^{o}C for six hours without signal degradation. The hydrophone specifications provided by the manufacturer state that the case material cannot withstand exposure to a hydrocarbon compound used in closed-loop geothermal production. The hydrophone was recovered from the well in August and replaced with a Shure PG58 vocal microphone hanging below the lip of the casing. The adhesive in the microphone element softened in the heat and humidity of the well casing, which significantly altered its sensitivity. The Shure PG58 microphone was recovered and replaced with a Rode NTG8 shotgun microphone, which was later replaced with another one, identically configured. The shotgun microphone was deployed with a windscreen and rubber isolation mount, aligned down the axis of the wellbore with the XLR connector on the back end at the lip of the casing. The Sound Devices 702 was powered by a pair of 110 amp-hour deep-cycle Absorbent Glass Mat (AGM) storage batteries charged by a photovoltaic array on the roof of the well enclosure. The data was written to an external hard drive or compact flash (CF) card. Though hard drives were available in capacities up to 2 TB, the write-speed would decrease as the hard drive filled. When the write-speed falls below the acquisition rate, the 702 pauses the recording. The CF cards, available in capacities up to 512 GB would bog down at about 127 GB, but CF media was ultimately favored because the hard drives caused electrical/RF interference with the USGS data-logger (even with the Sound Devices ® XHD filter, required more power, and having moving parts, were presumed more likely to fail in extreme seasonal temperatures and to reduce the required frequency of site visits to collect data.

Description of the Data

Analog audio recordings are a continuous time series of sound pressure level (spl), which is the instantaneous departure of the local fluid pressure from the ambient value caused by the incidence of a soundwave. Sound pressure level carries dimensions of pressure, and is conveyed in reference to an arbitrary amplitude of 20 micro-pascals. Taking the logarithm of the ratio of spl to the 20 micro-pascal reference yields acoustic power in decibels (dB). The spl value is recorded by the relative deflection of the microphone element from its equilibrium position. A digital audio recording is a series of discrete spl measurements, separated in time by intervals equal to the reciprocal of the sampling rate f_s (Hz). the voltage across the output terminals of the microphone scale with the relative deflection of the microphone element from its equilibrium position. The voltage at the microphone output is sampled and recorded every $1/f_s$. The number of possible spl values that a digital audio recorder can register is determined by the bit depth and is equal to two raised to the power of the bit depth. A 16-bit recorder can distinguish 2^{16} = 65,536 different levels of sound pressure, whereas a 24-bit recording split each of those 65,536 into 256 sublevels for a total of 2^{24} = 16,777,216 different levels of loudness across the dynamic range of the microphone element. Modern, professional-grade digital audio recorders are 16- or 24-bit, with sampling rates ranging from 32 – 192 kHz, selection of which requires careful consideration for long-duration remote field deployments. In addition to establishing the rate at which data is recorded, the bit depth *d*, and sampling rate determine the sensitivity to variations in *spl* and frequency resolution, respectively. The data rate (bits per second) is equal to the product of the sampling rate (measurements per second) and the bit depth (bits per measurement). Recording time per TB is shown in table 1 for a variety of bit depth and

sampling rate configurations. The human ear is tuned for sensitivity to frequencies in the 20 – 20,000 Hz range. Commercial audio microphones are designed to exhibit a linear relationship with spl and voltage output across that frequency range. The sampling rate also determines the highest frequency that can be captured in a recording. Known as the Nyquist frequency, or corner frequency, this upper limit is equal to half the sampling rate. Recordings were acquired in a laboratory column containing carbonated water, champagne, and still water brought gradually to a rolling boil. The complete set of recordings comprises nearly 10,000 hours of digital audio, more than 9000 hours, 1,350 tracks of recordings from CH-10B, a total of 41 TB of 1.66 GB .wav files, the complete description of which is shown in table 2. The data used in this analysis was acquired using two identical NTG8 microphones in a fixed position, with constant gain settings. This configuration captured eight M7+ events for which CH-10B water level data are available. Four of these eight events are analyzed in depth, including three that initiated a CH-10B water level response, and one that didn't. The epicenters of these events are mapped along with CH-10B in figure 7. Seismic data was collected from the Kaiser Creek (KCC) station of the Berkeley Digital Seismic Network (BDSN), located approximately 45 miles southwest from the CH10B well site. Data was downloaded in miniseed format from the Northern California Earthquake Data Center (NCEDC) (http://ncedc.org/). P-wave arrival times were estimated using the 'iasp91' 1D velocity model (*Kennett and Engdahl*, 1991] implemented in ObsPy, an open-source framework for processing seismological data in Python (https://docs.obspy.org/). Most of the acoustic power at CH-10B consists of low-frequency noise arising from wind, aircraft, and the deep gurgle of the gas-bubbler, electrical relays chattering inside the data-logger the casing, the Helmholtz resonance of the air column in the well casing (~1 Hz). A -60dB, 200 Hz low-cut filter was applied on the 702 subsequent to the 29 July 2016 event to attenuate the low-frequency noise, which made it possible to increase the microphone gain, significantly increasing mid- and high-frequency sensitivity and better bubble size statistics in the physical size range observed in prior laboratory experiments. The acoustic spectra of the three events that we analyze subsequent to turning on the filter show the effect of its application on the before and after plots, but doesn't affect the difference between after and before. Images of the hydrophone, Shure PG58, and NTG8 microphones, and the recording system are shown in figure 8.

Analytical method

The audio spectra in the hours before and after the arrival of a P-wave at CH-10B are decomposed by Discrete Time Fourier Transform (DTFT), exemplified in figure 9. The time-averaged audio spectrum before the P-wave arrival is subtracted from the initial one to resolve co-seismic changes in acoustic power. The frequency axis of the audio spectrum can then be correlated to gas bubble size distribution and the acoustic power associated with number density in the formation fluid. The DTFT interval should be long enough to capture at least one period of the lowest frequency signal, but not so long that relatively short-duration transient features of the audio spectrum are averaged out and suppressed. Audio frequency is inversely correlated to bubble radius using the relationship developed by *Minnaert* (1933).

Laboratory validation of the analytical method – boiling experiment

We recorded audio from 1.7 L of tap water in a glass kettle as it was heated from room temperature to a rolling boil, simultaneously using a hydrophone and a shotgun microphone, accompanied by digital video at 30 fps and 1080 dpi. As the water warms, the audio signal decreases in pitch as the gas bubbles increase in size. The effect is notable in the acoustic power spectrum. The first bubbles to appear have radii on the order of perhaps ~10-100 microns, growing to ~10^0 cm at a rolling boil – a change spanning three or so orders of magnitude in size, reflected in the relative shifts in the peak of the acoustic power spectrum. Frames from the boiling experiment video are arranged into four rows in figure 10,

corresponding to the four DTFT intervals into which it is segmented. The spectra and differences between the audio spectrum in the second, third and fourth DTFT intervals and the first one is shown in figure 11.

Discussion of results

Of the four M7+ event analyzed in this study, the three earthquakes that caused a CH-10B water level response were preceded by an increase in acoustic power in the 200-200 Hz band concurrent with the arrival of the P-wave. The coincidence (and co-absence) of the acoustic and water-level responses connotes a possible linkage between the two phenomena. The absence of a co-seismic response to the August 19, 2016 event (figure 12) is conspicuous next to the other three events that occurred at similar distances from CH-10B with comparable magnitudes and did cause the water level to drop (figures 13-15). The bearing of the epicenter in the August 19, 2016 earthquake to CH-10B is approximately perpendicular the San Andreas and Great Basin extensional range-front faults, whereas the other three events deliver energy to CH-10B roughly perpendicular to those fault networks and some of the regional flow groundwater flow systems. When broadband seismic energy is delivered parallel to the strike of a fault, shearing modes are activated, which cause no volumetric contraction or dilation, and cannot propagate through fluids. Seismic waves incident perpendicular to the strike of a fault activate compressive vibrational modes, which can drive gas phase into or out of solution. The character of the seismic spectrum varies between these events, with some very long-period shear waves appearing in the August 19, 2016 event. The ground velocity during this event has an amplitude that is approximately an order of magnitude smaller than the other three events, suggesting a greater dependence on the shear modulus than the elastic modulus. Helmholtz resonance and variations in the density and pressure of the gas column in the wellbore influence the audio spectrum. The frequencies of fundamental modes of such resonance can be approximated from theoretical formulae, but remain a source of uncertainty. Differential monitoring, where the spl from a microphone facing down the wellbore is compared to a simultaneous record of an upward facing one may be advantageous inasmuch as it would reduce the effort associated with developing and relying on a time-averaged audio fingerprint of the ambient noise environment. Dispersion of the audio signal is another source of uncertainty – sound waves with different frequencies are differentially attenuated and travel at slightly different speeds. This tends to suppress high frequencies and amplify the lower ones. Good resolution at high audio frequencies requires close proximity between the microphone and the source, which remains a challenge in the extreme conditions of CH-10B. Optical acoustics, like DTS cable, or Fabry-Perot etalon laser-interferometry may be viable alternatives to vocal microphones. Speed of sound measurements in the air column above the water surface, inferred from two-way travel time of a pulsed sound wave and the depth-to-water from the gas-bubbler can further enhance the acoustic spectral resolution by computing and graphically overlaying the frequencies of Helmoltz resonances and their harmonics.

Conclusions

Hardware and software configurations for recording, processing, analyzing and interpreting audio in a remote gas-rich hydrothermal borehole known to exhibit a co-seismic response were developed and refined over an 18-month period. Numerous seismic events were recorded, including several that initiated water level changes at CH-10B. The water level changes correlate with positive and negative deflections in the acoustic power in the 200-300 Hz band, coincident with the arrival of the P-wave, correlating to nucleation and extinction, respectively, of gas bubbles in the 10^0-10^1 mm size range. In instances where no water level change occurs at CH-10B, no acoustic response was observed, supporting a gas-phase-change mechanism for the water level response. We attribute the differing character of the water level response across seismic events bearing comparable energy density to variations in the pre-seismic reservoir fluid conditions, pressure history, and gas volume fraction in the near field of CH-10B. Gas –

phase CO_2 being the non-wetting fluid will preferentially enter and occupy larger pores, including the wellbore. Mobilization of entrapped gas by long-period seismic waves may increase the gas bubble rupture rate in the well. As gas phase vents from the wellbore to the atmosphere, the formation fluid pressure decreases – a potential mechanism for the CH-10B water level drop. Seismic motion imparted to CH-10B may act to consolidate small gas bubbles into larger ones, enhancing their mobility toward the well. If the formation fluid is saturated with respect to dissolved CO_2, the pressure drop initiates an aqueous-to-gas phase change, entrapping additional gas phase in the pore space, which slowly restores the pore fluid pressure.

Figures

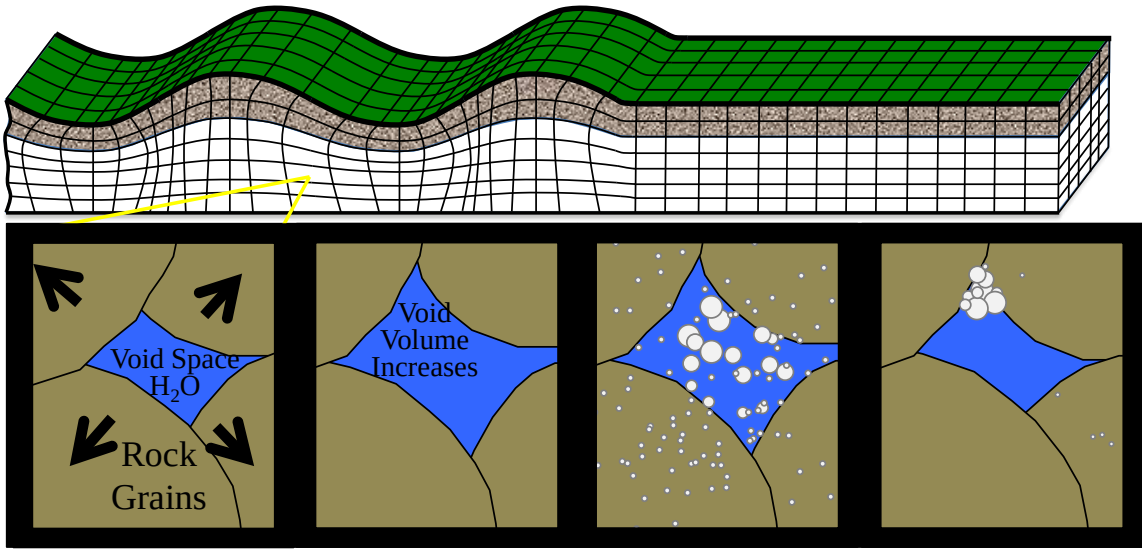

Figure 1. Conceptualization of a Rayleigh wave propagating through an aquifer containing water with a high concentration of dissolved CO_2. The Rayleigh wave locally compresses and expands the aquifer. The confining stress oscillation causes a proportional oscillation of the pore fluid pressure. During the expansion phase, the pore pressure falls below the bubble pressure, and CO_2 bubbles form in the pore space. After the Rayleigh wave passes, the CO_2 bubbles re-dissolve very slowly. Bubbles displace and compress the liquid in the pore space, resulting in a sustained increase in pore fluid pressure and reduction of effective stress.

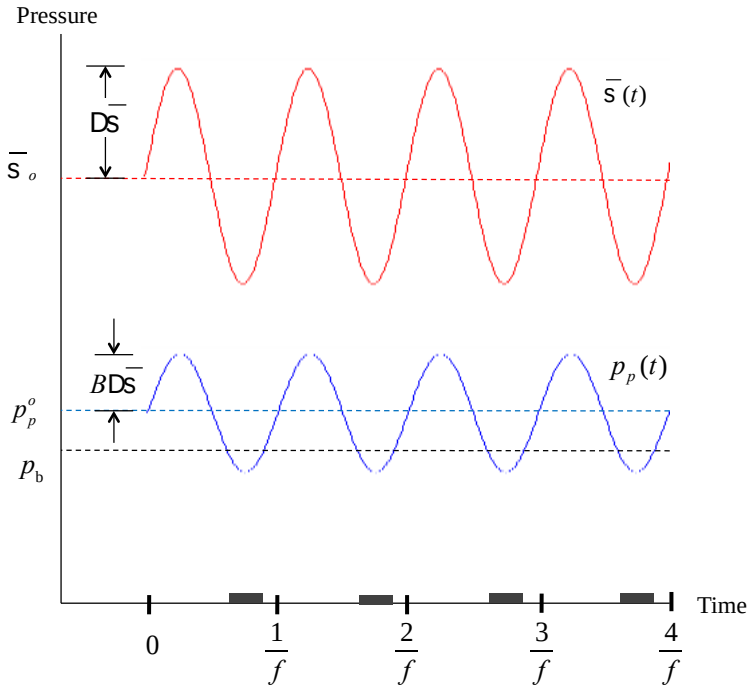

Figure 2. Conceptual plot of a sinusoidal confining stress oscillation (red) and the pore pressure response (blue). The amplitude of the pore pressure oscillation is scaled by Skempton's coefficient, *B*. If the pore pressure falls below the bubble pressure during some portion of the oscillation cycle, CO_2 gas bubbles will nucleate and grow in the pore space.

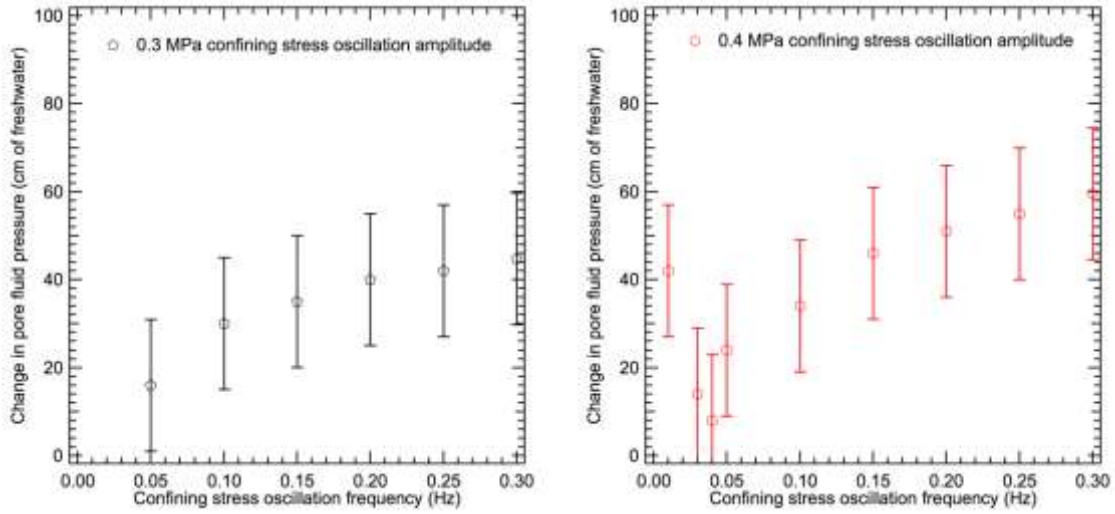

Figure 3. Pore pressure increase measured due to CO_2 bubble growth in a Berea sandstone core flooded with high-CO_2 water and subjected to confining stress oscillations at frequencies and amplitudes representative of the dynamic stress imposed on LVC by the June 28, 1992 Landers, CA, earthquake Rayleigh wave. For comparison, the water level in the CW-3 well in LVC rose 41.8 cm in response to the Landers Rayleigh wave. The response in the Berea core increases with confining stress amplitude and frequency [*Crews and Cooper*, 2014b].

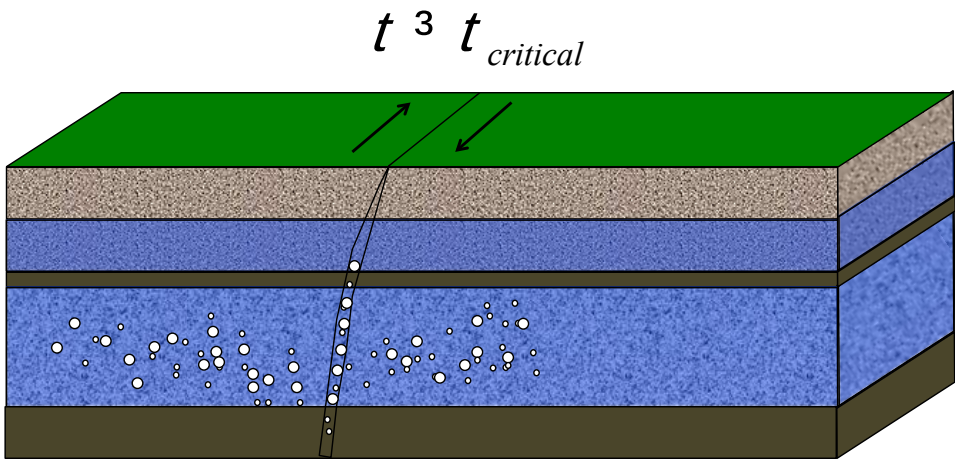

Figure 4. Conceptual drawing of CO_2 gas bubble nucleation and growth in and near a critically stressed fault, as a mechanism for remotely triggered seismicity. A distant earthquake radiates a Rayleigh wave through a fault and adjacent aquifer, which contain water with a high concentration of dissolved CO_2. Bubble nucleation and growth occur in the pore space and in water-saturated portions of the fault. Diffusion of elevated pore fluid pressure into the fault results in a reduction of effective stress and a lowering of the critical shear stress required to initiate fault movement.

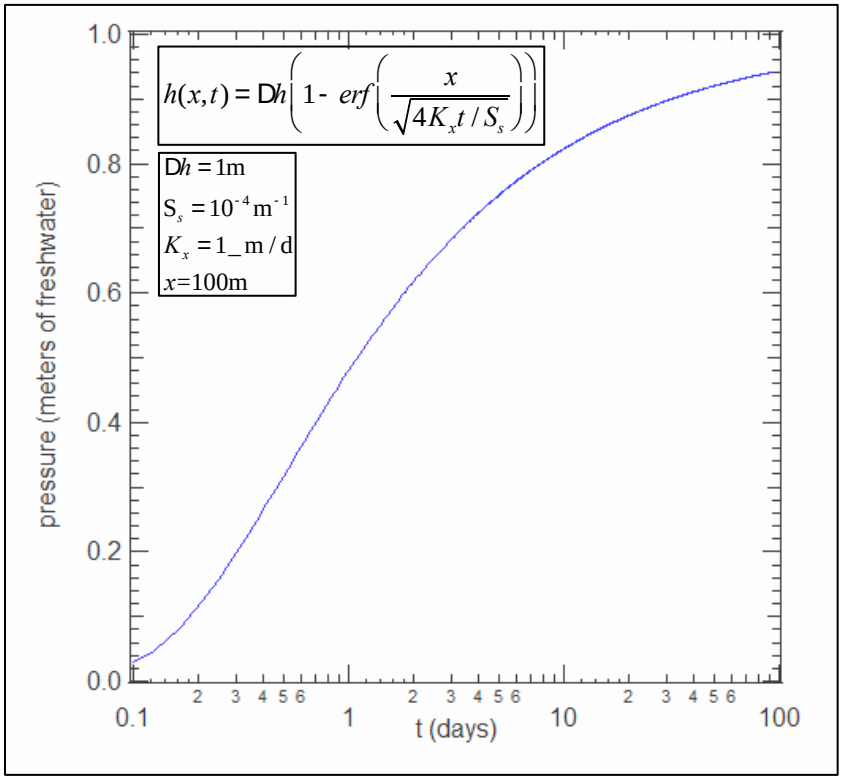

Figure 5. Plot of the 1-D solution to the groundwater flow equation describing the diffusion of a 1 m head increase caused by the seismically initiated nucleation and growth of CO_2 bubbles in a confined aquifer to an observation point 100 m away. After 36 hours, approximately 50 percent of the head increase is communicated to the observation point. This diffusive behavior may account for the time delays observed between induced seismic events and the triggering event.

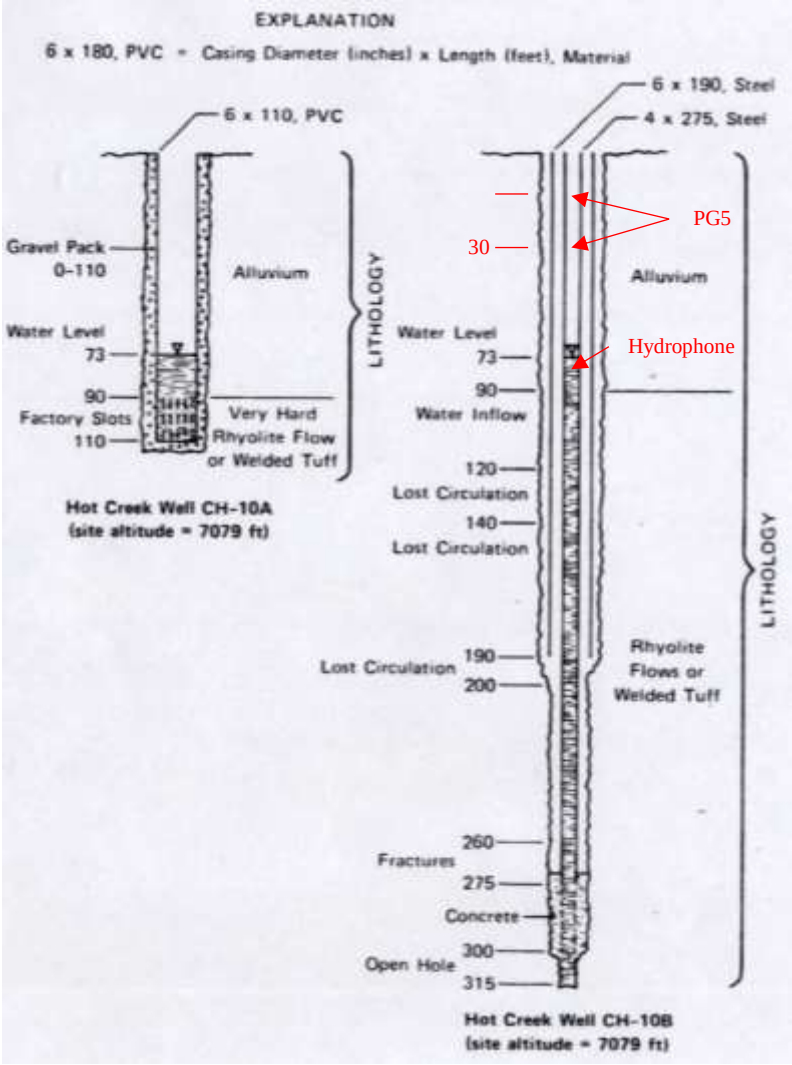

Figure 6. Photograph and Schematic of the well construction at CH-10B, and neighboring CH-10A.

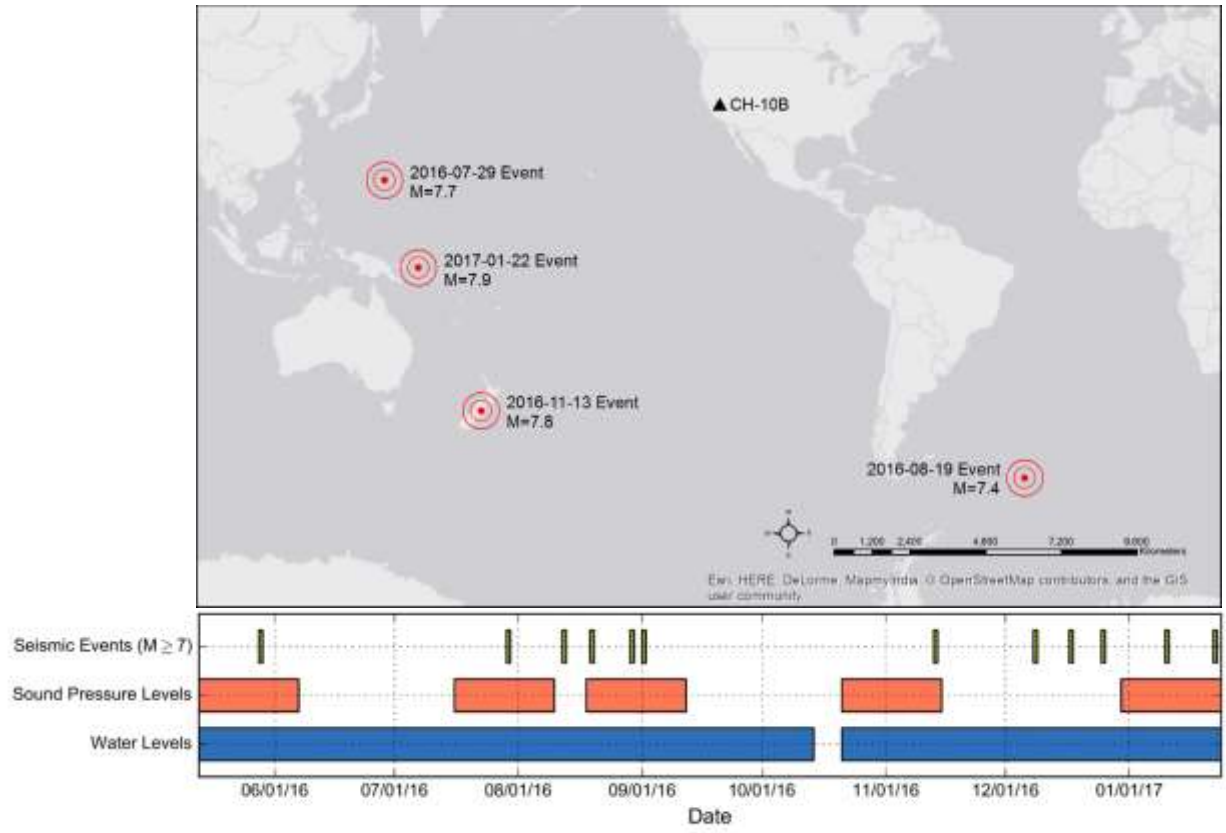

Figure 7. Data coverage and map of seismic events analyzed in the present study, showing locations in relation to CH-10B. While the recordings at CH-10B began on June 18, 2015, the interval shown in the figure is spanned by a consistent configuration of the recording system, which facilitates direct comparison of the CH-10B acoustic response across different seismic events.

Figure 8. Photographs of the hydrophone (left), water-damaged PG58 microphone element (top center), Sound Devices 702 recorder (bottom center), and the configuration of equipment inside the well house using the NTG8 shotgun microphone, the black rubber suspension mount of which is visible in the top of the borehole (right).

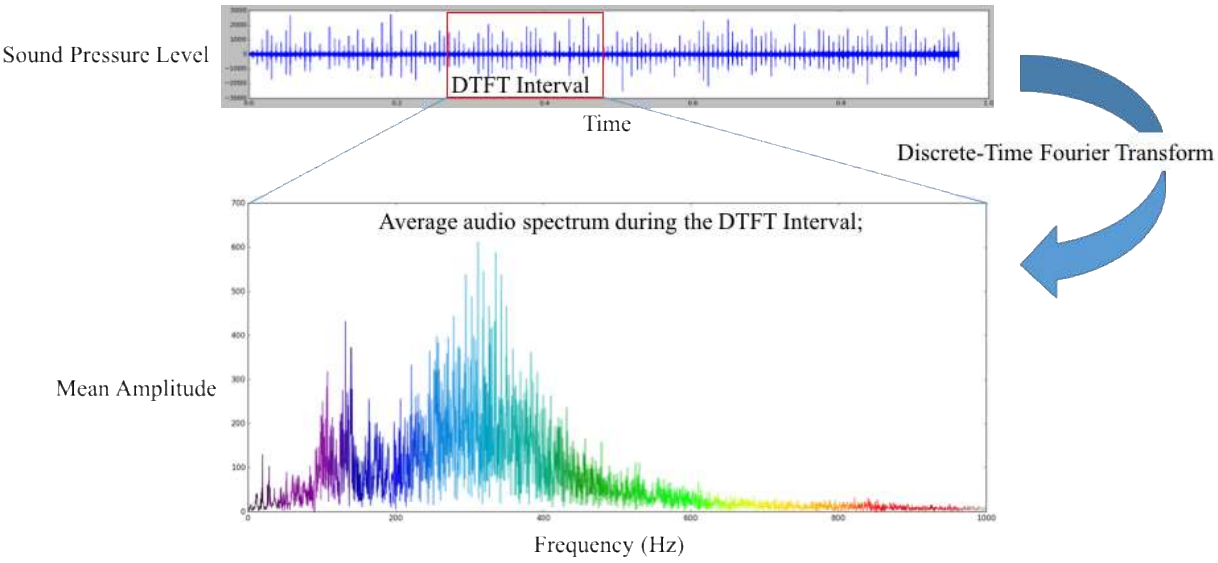

Figure 9. Plot of sound pressure level record and its audio spectrum obtained from a Discreet-Time Fourier Transform.

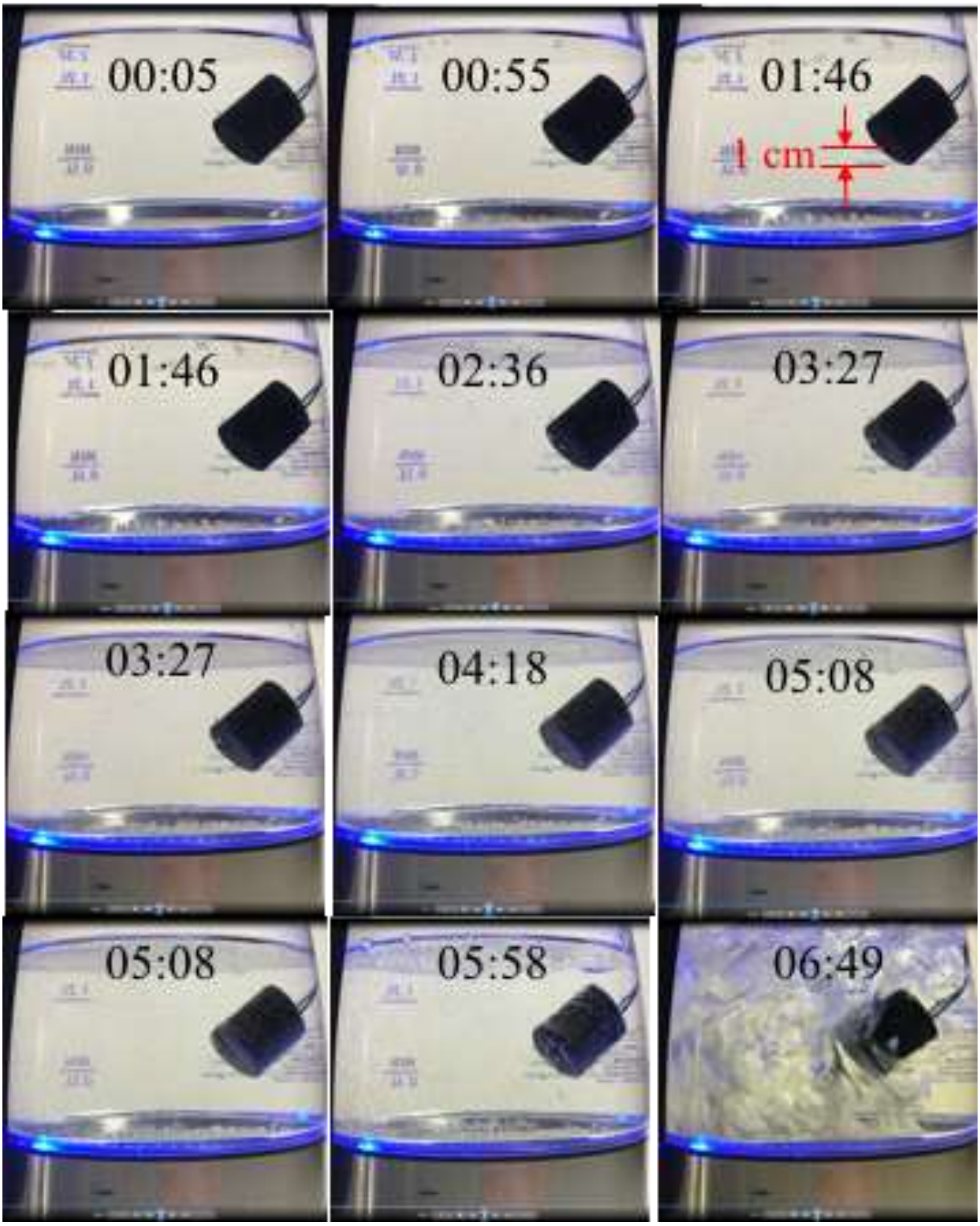

Figure 10. Frames from a video of 1.7 L of water brought from room-temperature to a rolling boil, recorded with a hydrophone and the NTG8 shotgun microphone.

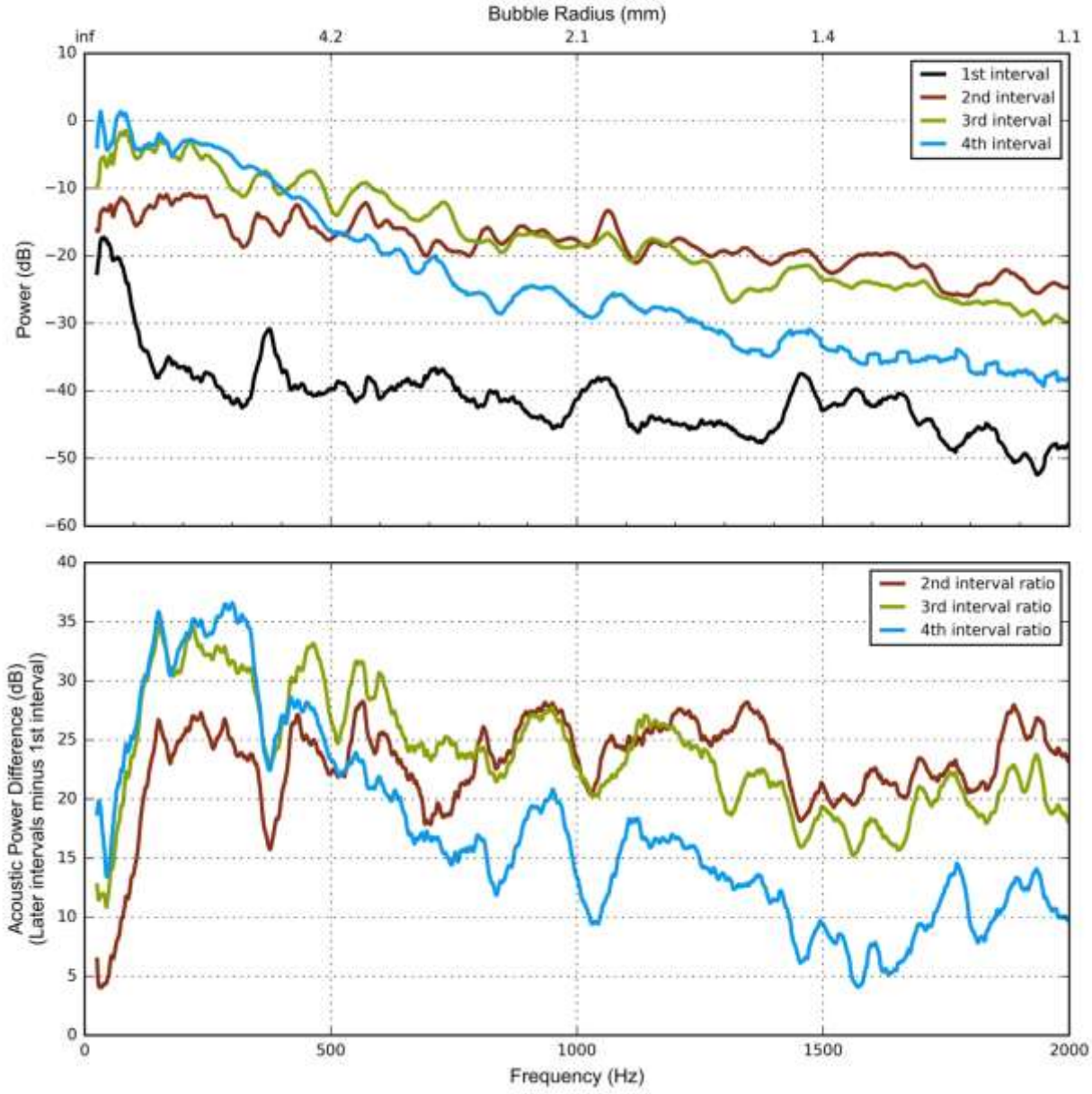

Figure 11. Audio spectra for the four time intervals of the boiling experiment, corresponding to the rows of images in figure 10. As boiling intensifies, the low-frequency components increase in amplitude, while the higher frequency components tend to weaken.

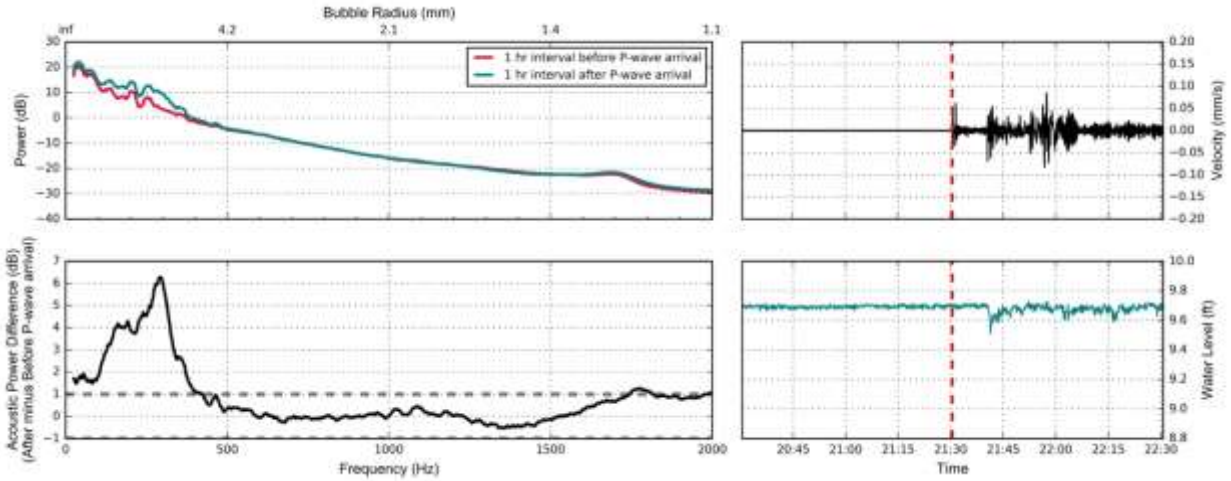

Figure 12. Acoustic spectra in the hours before and after the 29 July, 2016 M7.7 (top left), the difference between them (bottom left), the ground velocity (top right), and CH-10B water level (bottom right), with the P-wave arrival indicated by a vertical red dashed line. The low-frequency before and after spectra are unfiltered in the upper-left plot. A 60dB low cut filter was subsequently applied at 20-200 Hz.

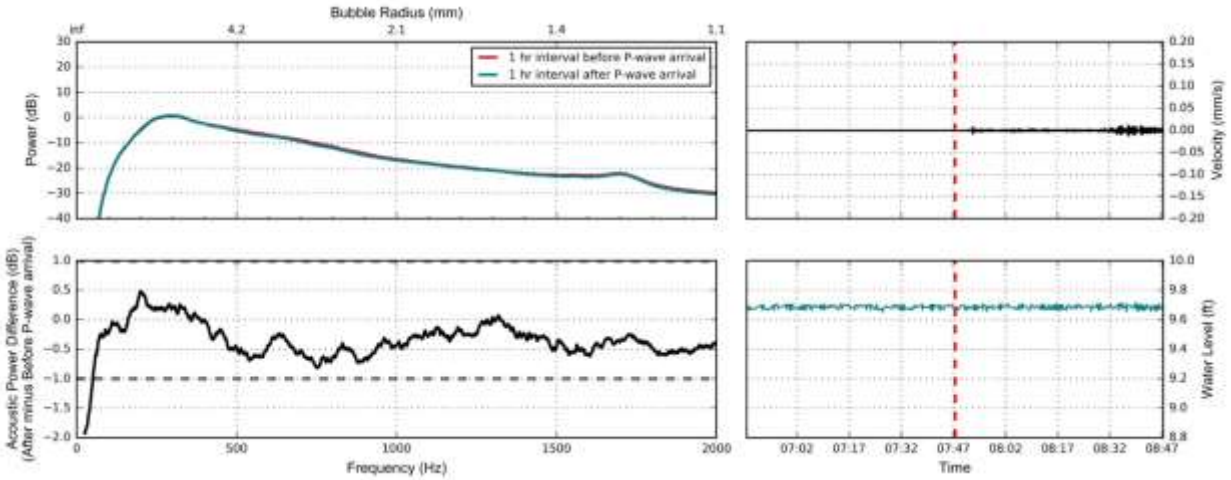

Figure 13. Acoustic spectra in the hours before and after the 19 August, 2016 M7.4 (top left), the difference between them (bottom left), the ground velocity (top right), and CH-10B water level (bottom right), with the P-wave arrival indicated by a vertical red dashed line.

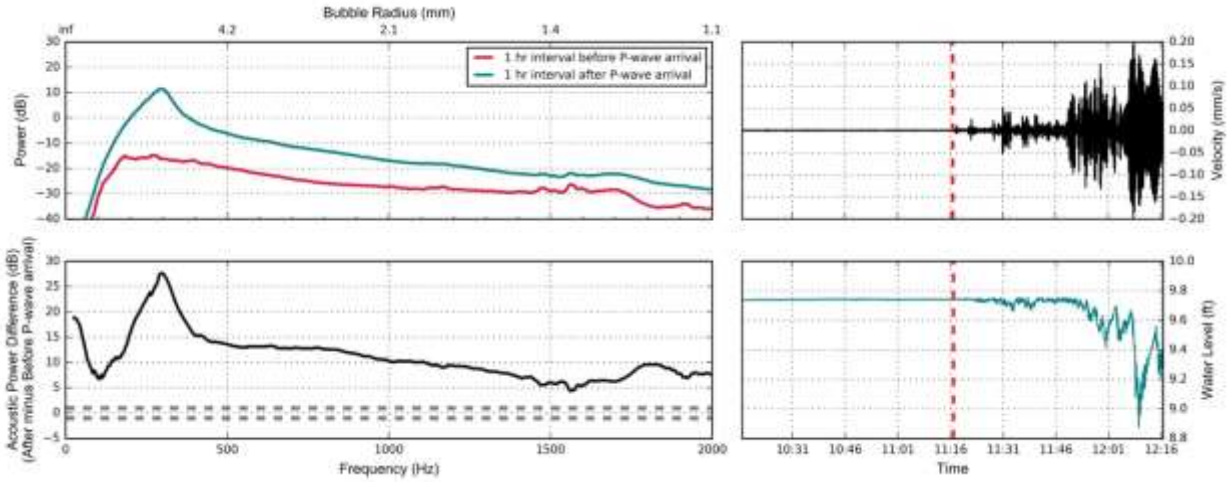

Figure 14. Acoustic spectra in the hours before and after the 13 November, 2016 M7.8 (top left), the difference between them (bottom left), the ground velocity (top right), and CH-10B water level (bottom right), with the P-wave arrival indicated by a vertical red dashed line.

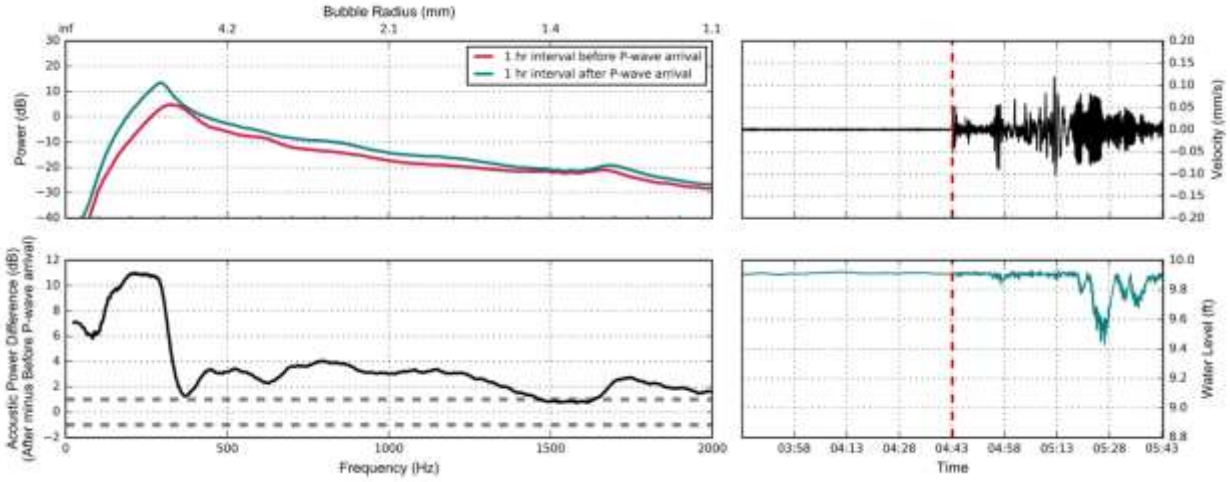

Figure 15. Acoustic spectra in the hours before and after the 22 January, 2017 M7.9 (top left), the difference between them (bottom left), the ground velocity (top right), and CH-10B water level (bottom right), with the P-wave arrival indicated by a vertical red dashed line.

Tables

Table 1. Maximum recording time in days-per-TB for a single-channel at various combinations of bit-depth and sampling-rate.

		Sampling Rate (kHz)							
		32	44.1	47.952	48	88.2	96	176.4	192
Bit Depth	16	180	131.5	123	120	65	60	32	30
	24	120	87	82	80	43	40	21	20

Recording Time (days / TB)

Table 2. Complete description of the audio recordings from CH-10B, including hardware and recording configurations (available as a digital supplement).

Bibliography of work published under this award

Crews, J. B., 2015, *Acoustic monitoring of co-seismic changes in gas bubble rupture rate in a hydrothermal reservoir: a possible precursor and mechanism for remote seismic triggering,* Proceedings of the American Geophysical Union Fall Conference, San Francisco, CA, S12A-05.

Crews, J. B., 2015, *Carbon dioxide gas bubble growth in groundwater: A mechanism for remote earthquake triggering,* Invited talk – Presented to the USGS National Earthquake Hazards Reduction seminar series, Menlo Park, CA, June 10, 2015.

References

Barnes, I., W. P. Irwin, and D. E. White (1984) Global distribution of carbon dioxide discharges and major zones of seismicity, *USGS Water-Resources Investigations Report.*

Bear, J. (1988) *Dynamics of Fluids in Porous Media*, Dover Publications Inc., New York, United States. Reprint of 1972 Elsevier, Edition.

Bergfeld, D., W. C. Evans, J. F. Howle, and C. D. Farrar (2006) Carbon dioxide emissions from vegetation-kill zones around the resurgent dome of Long Valley caldera, eastern California, USA, *Journal of Volcanology and Geothermal Research, 152*, 140-156, doi: 10.1016/j.jvolgeores.2005.11.003.

Bergfeld, D., F. Goff, and C. J. Janik (2001) Elevated carbon dioxide flux at the Dixie Valley geothermal field, Nevada: Relations between surface phenomena and the geothermal reservoir, *Chem. Geol., 177*, 43-66, doi: 10.1016/S0009-2541(00)00381-8.

Biot, M. A. (1956) Theory of propagation of elastic waves in a fluid-saturated porous solid, part 1, *Acoustic Society of America, 28,* 168-179.

Brodsky, E. E., E. Roeloffs, D. Woodcock, I. Gall, and M. Manga (2003) A mechanism for sustained groundwater pressure changes induced by distant earthquakes, *Journal of Geophysical Research, 108*(B8), 2390, doi: 10.1029/2002JB002321.

Brown, S. T., B. M. Kennedy, D. J. DePaolo, S. Hurwitz, and W. C. Evans (2013) Ca, Sr, O and D isotope approach to defining the chemical evolution of hydrothermal fluids: Example from Lang Valley, CA, USA, *Geochimica et Cosmochimica Acta, 122*, 209-225.

Carslaw, H. S., and J. C. Jaeger (1959) *Conduction of heat in solids*, 2nd Ed., Oxford, Clarendon Press.

Crews, J. B. and C. A. Cooper, 2014, Experimental evidence for seismically initiated gas bubble nucleation and growth in groundwater as a mechanism for coseismic borehole water level rise and remotely triggered seismicity, *Journal of Geophysical Research – Solid Earth, 119*(9), 7079-7091, doi: 10.1002/2014JB011398.

Crews, J. B. and C. A. Cooper, 2014, Transient pore pressure response to confining stress excursions in Berea sandstone flooded with an aqueous solution of CO2, *Water Resources Research, 50*, doi: 10.1002/2014WR015305.

Diamond, L. W. and N. N. Akinfiev (2003), Solubility of CO_2 in water from -1.5 to 100^oC and from 0.1 to 100 MPa: Evaluation of literature data and thermodynamic modeling, *Fluid Phase Equilibria, 208*, 265-290, doi:10.1016/S0378-3812(03)00041-4.

Elkhoury, J. E., E. E. Brodsky, and D. C. Agnew (2006) Seismic waves increase permeability, *Nature, 441*, 1135-1138, doi: 10.1038/nature04789.

Elkhoury, J. E., A. Niemeijer, E. E. Brodsky, and C. Marone (2010) Dynamic stress stimulates flow in fractures: laboratory observations of permeability enhancement, *Journal of Geophysical Research, 115*.

Elkhoury, J. E., ., A. Niemeijer, E. E. Brodsky, and C. Marone (2011) Laboratory observations of permeability enhancement by fluid pressure oscillation of in situ fractured rock, *Journal of Geophysical Research, 116*.

Ellsworth, W. L. (2013) Injection-induced earthquakes, *Science, 341*, 142-151, doi: 10.1126/science.1225942

Farrar, C. D., M. L. Sorey, W. C. Evans, J. F. Howle, B. D. Kerr, B. M. Kennedy, C.-Y. King, and J. R. Southon (1995) Forest-killing diffuse CO_2 emission at Mammoth Mountain as a sign of magmatic unrest, *Nature, 376*, 675-678, doi: 10.1038/376675a0.

Freed, A. M. (2005) Earthquake triggering by static, dynamic, and postseismic stress transfer, *Annual Review of Earth and Planetary Science, 33*, 335-367.

Geertsma, J. and D. C. Smit (1961) Some aspects of elastic wave propagation in fluid-saturated porous solids, *Geophysics, 26*(2), 169-181.

Gomberg, J., P. Bodin, and P. A. Reasenberg (2003) Observing earthquakes triggered in the near field by dynamic deformations, *Bulletin of the Seismological Society of America, 93*(1), 118-138.

Hill, D. P., P. A. Reasenberg, A. Michel, W. J. Arabaz, G. Beroza, D. Brumbaugh, J. N. Brune, R. Castro, S. Davis, D. dePolo, W. L. Ellsworth, J. Gomberg, S. Harmsen, L. House, S. M. Jackson, M. J. S. Johnston, L. Jones, R. Keller, S. Malone, L. Munguia, S. Nava, J. C. Pechmann, A. Sanford, R. W. Simpson, R. B. Smith, M. Stark, M. Stickney, A. Vidal, S. Walter, V. Wong, and J. Zollweg (1993) Seismicity remotely triggered by the 7.3 Landers, California, earthquake, *Science, 260*(5114), 1617-1623, doi: 10.1126/science.260.5114.1617.

Hill, D. P., and S. G. Prejean (2006) *Treatise on Geophysics*, G. Shubert ed., also Ch. 8 vol. 4 of *Earthquake Seismology*, H. Kanamori ed.

Hubbert, M. K. and W. W. Rubey (1959) Role of fluid pressure in mechanics of overthrust faulting, *Geological Society of America Bulletin, 70*(2), 115-166, doi: 10.1130/0016-7606(1959)70[115:ROFPIM]2.0.CO;2.

Husen, S., S. Wiemer, and R. B. Smith, (2004) Remotely triggered seismicity in the Yellowstone National Park region by the 2002 Mw 7.9 Denali Fault earthquake, Alaska, *Bulletin of the Seismological Society of America*, *94*, 317-331.

Ichihara, M., and E. E> Brodsky (2006) A limit on the effect of rectified diffusion in volcanic systems, *Geophysical Research Letters, 33*(2), L02316, doi: 10.1029/2005GL024753.

Irwin, W. P., and I. Barnes (1980) Techtonic relations of carbon dioxide discharges and earthquakes, *Journal of Geophysical Research, 85*, 3115-3121.

Jones, S.F., G.M. Evans, K.P. Galvin (1999) Bubble nucleation from gas cavities – a review, *Advances in Colloid and Interface Science, 80,* 27-50.

Jónsson, S. P. Segall, R. Pedersen, and G. Bjornsson (2003) Post-earthqauke ground movements correlated to pore-pressure transients, *Letters to Nature*, *424*, 179-183.

Kennett, B. L. N. and Engdahl, E. R. (1991), Traveltimes for global earthquake location and phase identification, *Geophysical Journal International*, 105 (2), 429-465. https://dx.doi.org/10.1111/j.1365-246X.1991.tb06724.x

Kerrick, D. M. (2001) Present and past nonanthropogenic CO_2 degassing from the solid Earth, *Reviews of Geophysics, 39(4),* 565-585, doi: 10.1029/2001RG000105.

Lewicki, J. L. and S. L. Brantley (2000) CO_2 degassing along the San Andreas fault, Parkfield, California, *Geophysical Research Letters*, *27*, 5-8, doi: 10.1029/1999GL008380.

Linde, A. T., I. S. Sacks, M J. S. Johnston, D. P. Hillt, and R. Bilham (1994) Increased pressure from rising bubbles as a mechanism for remotely triggered seismicity, *Nature, 371*, 408-410, doi: 10.1038/371408a0.

Lowrie, W. (1997) *Fundamentals of Geophysics*, Cambridge University Press, Cambridge, United Kingdom.

Manga, M., I. Beresnev, E. E. Brodsky, J. E. Elkhoury, D. Elsworth, S. E. Ingebritsen, D. C. Mays, and C. Wang (2012) Changes in permeability caused by transient stresses: Field observations, experiments, and mechanisms, *Reviews of Geophysics, 50.*

Manga, M., and E. Brodsky (2006) Seismic triggering of eruption in the far field: Volcanoes and Geysers, *Annual Review of Earth and Planetary Science, 34,* 263-291.

Nielsen, L. C., I. C. Bourg, G. Sposito (2012) Predicting CO_2-water interfacial tension under pressure and temperature conditions of geologic CO_2 storage, *Geochimica et Cosmochimica Acta, 81,* 28-38, doi: 10.1016/j.gca.2011.12.018.

Pankow, K. L., Arabasz, W. J., Pechmann, J. C. and Nava, S. J. 2004 Triggered seismicity in Utah from the 3 November 2002 Denali Fault earthquake, *Bulletin of the*

Seismological Society of America, 94, 332-347.

Prejean, S. G., Hill, D. P., Brodsky, E. E., Hough, S. E., Johnston, M. J. S., Malone, S. D., Oppenheimer, D. H., Pitt, A. M. and Richards-Dinger, K. B. (2004) Remotely triggered seismicity on the United States west coast following the Mw 7.9 Denali Fault earthquake, *Bulletin of the Seismological Society of America, 94*, 348-359.

Minnaert, M. (1933) On musical air-bubbles and the sound of running water, *Philosophical Magazine*, 16 (104): 235–248, doi:10.1080/14786443309462277

Roeloffs, E. A., W. R. Danskin, C. D. Farrar, D. L. Galloway, S. N. Hamlin, E. G. Quilty, H. M. Quinn, D. H. Schaefer, M. L. Sorey, and D. E. Woodcock (1995) Hydrologic effects associated with the June 28, 1992 Landers, California, earthquake sequence, *U. S. Department of the Interior United States Geologic Survey Open File Report*, 95-42.

Roeloffs, E. A. (1998) Persistent water level changes in a well near Parkfield, California due to local and distant earthquakes, *Journal of Geophysical Research, 103*(B1), 869-889, doi: 10.1029/97JB02335.

Roy, J. W., and M. C. Ryan (2010) In-well degassing issues for measurements of dissolved gases in groundwater, *Ground Water, 48*(6), 869-877, doi: 10.1111/j.1745-6584.2010.00703.x.

Skempton, A. W. (1954) The pore-pressure coefficients A and B, *Geotechnique, 4*, 143-147, doi: 10.1680/geot.1954.4.4.143.

Sturtevant, B., H. Kanamori, and E. E. Brodsky (1996) Seismic triggering by rectified diffusion in geothermal systems, *Journal of Geophysical Research, 101*, 25269-25282.

Wang, R., H. Woith, C. Milkerieit, and J. Zschau (2004) Modeling of hydrogeochemical anomalies induced by distant earthquakes, *Geophisical Journal International, 157,* 717-726, doi: 10.111/j.1365-246x.2004.02240.x.

Weinlich, F. H. (2014) Carbon dioxide controlled earthquake distribution pattern in the NW Bohemian swarm earthquake region, western Eger Rift, Czech Republic – gas migration in the crystalline basement, *Geofluids*, *14*, 143-159, doi: 10.1111/gfl.12058.

Zones, C. P. (1957) Changes in hydrologic conditions in the Dixie Valley and Fairview Valley areas, Nevada, after the earthquake of December 16, 1954, *Bulletin of the Seismological Society of America, 47,* 387-396.